REVIEW ARTICLE

The anatomy of the rat eye with oxygen-induced retinopathy

**James D. Akula · Tara L. Favazza · Julie A. Mocko ·
Ilan Y. Benador · Ana L. Asturias · Michael S. Kleinman ·
Ronald M. Hansen · Anne B. Fulton**

Abstract Prior studies have documented the intertwined developmental courses of retinal blood vessel tortuosity (in fundus photographs) and retinal dysfunction (in electroretinographs) in Sprague–Dawley rat models of retinopathy of prematurity (ROP). Two such models, the "50/10 model" and the "75 model," are named after the oxygen regimens used to induce retinopathy and are characterized by distinct neurovascular courses that span a range of disease severity. In this study of 50/10 and 75 model rats, retinal flatmounts were used to study the full vasculature at postnatal day (P) 15, P19 and P30. In addition, the layers of the neural retina were measured in toluidine blue-stained cross sections. Finally, gross anatomic features of the eye, including axial length, retinal surface area, and the ratio of anterior to posterior axial-lengths were evaluated. Both clock hours of neovascularization (NV) and percent avascular retina (AR) peaked at P19 and resolved by P30. Through P19, NV was found in every 50/10 model rat, but in only 60% of 75 model rats. AR was positively related to NV. All inner layers of the retina (outer plexiform layer through ganglion cell layer) were attenuated in 50/10 model rats but, in the 75 model, no layer differed significantly from that in controls. The eyes in both ROP models were smaller than those of age-matched controls. The ratio of anterior to posterior axial-lengths ranged from 0.45 in controls through 0.37 in the 75 model to 0.32 in the 50/10 model. Thus, eye growth is altered in these rat models of ROP.

Keywords Retinopathy of prematurity ·
Rat · Angiogenesis · Anatomy · Refractive
development · Histology · Retina

J. D. Akula (✉) · T. L. Favazza · J. A. Mocko ·
I. Y. Benador · A. L. Asturias · M. S. Kleinman ·
R. M. Hansen · A. B. Fulton
Department of Ophthalmology, Fegan 4, Children's
Hospital Boston, Boston, MA 02115, USA
e-mail: ximtc@yahoo.com

J. D. Akula · R. M. Hansen · A. B. Fulton
Department of Ophthalmology, Harvard Medical School,
Boston, MA 02115, USA

Introduction

The incidence and severity of retinopathy of prematurity (ROP) in middle income countries is near all-time highs [1]. Worldwide, at least 50,000 children are binocularly blind, many times that number monocularly blind, and many fold again suffering from lifelong visual impairment as a consequence of ROP [1, 2]. In addition, the best currently available management of ROP involves indentifying high-risk vascular morphologies (i.e., dilated venules and tortuous arterioles at the posterior pole) early, and then ablating the avascular peripheral retina with a laser [3], an intervention that itself carries a certainty of lasting peripheral visual dysfunction. It follows

that new approaches to prevention and treatment of ROP are needed. Thus, this issue of *Documenta Ophthalmologica* dedicated to "the ROP rat" is timely.

ROP presents as abnormal retinal blood vessels in an ophthalmoscopic exam of the neonatal ocular fundus. Rat pups exposed to select alternating (relatively) high and low oxygen during the first days after birth develop a retinopathy that models human ROP. Such oxygen-induced retinopathy (OIR) is, therefore, a convenient in vivo model in which to study ROP.

Of particular significance, recent work in the ROP rat has demonstrated important interactions between the abnormal retinal vasculature that is the clinical hallmark of ROP and concomitant alterations in retinal function. For instance, in rat models of ROP, rod dysfunction antedates [4] and predicts [5] the subsequent retinal vascular abnormalities, while also persisting after their resolution [5, 6]. Meanwhile, postreceptor sensitivity recovers hand-in-hand with resolution of the retinal vascular abnormalities [5–7]. Indeed, the retinal vasculature and the postreceptor neural retina are in close physical proximity, are immature at the same ages, and develop under the cooperative control of growth factors that direct both angiogenesis and neurogenesis [7]. Thus, ROP is a neurovascular disease [8]. Furthermore, the postreceptor neural retina is principally supplied by the retinal vasculature that traverses the inner retinal surface, and thus is ideally situated to mediate the rod-vasculature relation. The postreceptor retina may be more susceptible to OIR [9], and postreceptor remodeling is associated with elevated levels of pro-angiogenic growth factors [7]. Since it is increasingly understood that the neural retina plays a prominent role in regulating eye growth [10, 11], it is unsurprising that eye growth and refractive development are commonly perturbed in children with a history of ROP [12–17].

In our recent investigations of the neurovascular relation in ROP rats, we have assessed the retinal vascular abnormalities using image analysis of digital photographs of the ocular fundus, manually [6] or by computer [5, 7]. Such a noninvasive approach has the notable advantage of allowing longitudinal assessment of the retinal vasculature. When used in conjunction with the electroretinogram (ERG), serial in vivo study of the neurovascular relation is possible.

However, neither fundus photography nor ERG provide detailed structural information about the neurovascular relation in OIR. Therefore, we have undertaken such a study in two ROP rat models that produce a range of severity in both vascular abnormality and neural dysfunction, the so-called "50/10" [18] and "75" [5] models, following a cross-sectional design. We have considered features from the thicknesses of the retinal layers to the coverage of the retinal blood vessels. We have also considered these features in the context of changes to the growth of the eye, and of earlier-obtained functional and molecular results.

Methods

Subjects

All studies were undertaken in Sprague–Dawley albino rats (Charles River Laboratories Inc., Worcester, MA). Rats were assigned to one of three groups, either of two OIR paradigms or room-air-reared controls. Because different rats contributed eyes to one or more of the several anatomic assessments listed below, numbers of rats utilized for each are given in the appropriate section below. The rats were sacrificed either by asphyxiation with CO_2 gas or by overdose of pentobarbital (~ 100 mg kg^{-1}). All experiments were conducted according to the ARVO Statement for the Use of Animals in Ophthalmic and Vision Research and with the approval of the Animal Care and Use Committee at Children's Hospital Boston.

Induction of retinopathy

We have previously described the OIR paradigms in detail [5]. Briefly, pups and dam were placed in an OxyCycler (Biospherix Ltd., Lacona, NY) and exposed to one of two different oxygen regimens at ages when the neural retina and its vasculature were immature. To produce the 50/10 model [18], pups were exposed to alternating 24 h periods of 50% and 10% oxygen beginning on postnatal day (P) 0 and lasting 2 weeks. To produce the 75 model, pups were exposed to 75% oxygen beginning on P7 and lasting 1 week. Thus, in both paradigms, pups were returned to room air (21% oxygen) on P14. Exposures similar to the 50/10 model reliably produce tortuosity of the

posterior retinal arterioles [5, 6] and peripheral neovascularization (NV) [19]. Exposures similar to the 75 model do reliably produce tortuosity of the posterior retinal vasculature [5, 7], but pervasive peripheral NV is not reported [20, 21].

Analysis of retinal vessels

The retinal blood vessels were studied in flatmounts of the whole retina. Prior to preparation of these flatmounts, the fundi of most of these eyes had been photographed using a RetCam equipped with an 'ROP lens' (Clarity Medical Systems Inc., Dublin, CA). In these cases, several images were composited (Photoshop CS3; Adobe Systems Inc., San Jose, CA) to create a view of the posterior pole, defined as the region within the circle bounded by the vortex veins and concentric to the optic nerve head (ONH). After imaging, the rats were sacrificed and their eyes enucleated and fixed in 4% paraformaldehyde for 20–30 min. Then, the corneas were incised and the lenses removed, and the retinae fixed for an additional hour in situ. The retinae were then isolated, intact, transferred to 1 mM $CaCl_2$ in PBS, and stained overnight at 23° C with 1:100 dilution fluoresceinated Griffonia Bandereiraea Simplicifolia Isolectin B4

(Alexa Fluor 594; Invitrogen, Carlsbad, CA). The retinae were then washed for 3 h in 1 × PBS, cut nearly into quadrants to allow them to lay flat, placed onto microscope slides, treated with SlowFade antifade reagent (Invitrogen), and coverslipped. Images were obtained by fluorescence microscopy (DM5500 microscope; Leica, Wetzlar, Germany) using an auto-tiling procedure to capture the entire retinal surface and a montaging algorithm (Photoshop "Photomerge" function) to create a single, high-resolution image of the retina.

As shown in Fig. 1, on the images of the flatmounted retinae, the boundary between the posterior pole and peripheral retina was demarked by identifying the position of the vortex veins using vascular landmarks identifiable in the fundus photographs. The percentage of avascular retina (AR) in the posterior and peripheral regions was quantified by comparing the number of pixels in the avascular areas with the total number of pixels in each region (ImageJ; W. S. Rasband, NIH, Bethesda, MD, http://rsb.info.nih.gov/ij/) [22]. In addition, the number of clock hours (CH) containing AR or NV were counted.

Flatmounts were obtained at one of three test ages (P15-16, P19 ± 1, P30 ± 1), from a total of 44 rats. The fundi of 30 of these rats were imaged with a
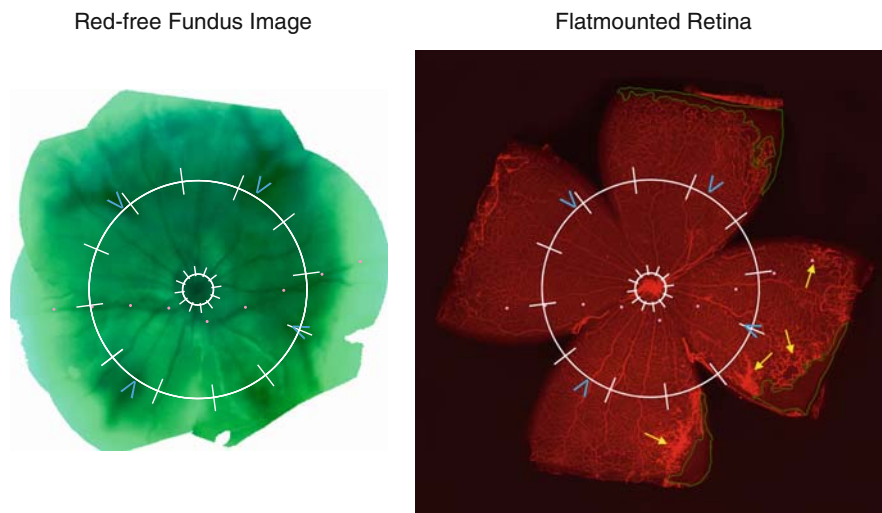

Red-free Fundus Image   Flatmounted Retina

Fig. 1 An image of the ocular fundus of a 50/10 model rat at P15 obtained with a digital fundus camera (left) and the same retina after flatmounting (right). Features such as the optic nerve head (small circle), vortex veins (blue Vs) and horizontal meridional line (dots) visible in the fundus image are used to determine the boundary between posterior and peripheral retina (large circle) and orient a clock face (ticks). Comparison of vascular landmarks allows approximate positioning of these features in the retinal flatmount, where avascular retina (green boundaries) and neovascularization (yellow arrows) are observed and quantified

RetCam prior to analysis and the landmarks used to facilitate orientation. The rats were divided nearly evenly across age and group (50/10 model, 75 model, control).

Histology

Eyes were prepared for histological assessment of the neural retina as follows: the corneas were incised, the lenses removed, and the retinae fixed by immersion of the eyes in Karnovsky's solution (5% glutaraldehyde, 4% paraformaldehyde). Orientation was preserved with a suture through the lateral rectus muscle. The fixed tissue was osmicated (1% osmium tetroxide, 1.5% potassium ferrocyanide) then placed in 1% uranyl acetate, dehydrated in graded cold alcohols, and infiltrated with 1:1 propylene oxide and resin (Taab 812) overnight before embedding in pure resin the following day. Thick sections (0.5 μm) were cut, placed on glass slides, and stained with 1% toluidine blue. Sections were obtained from four retinal regions (just superior and inferior to the ONH, and from the superior and inferior periphery) by first cutting the eye in half at the optic nerve along the horizontal meridian and then cutting two 2 mm × 4 mm sections from each half immediately adjacent to the initial cut and at 70–80% of the distance from the ONH to the *ora serrata*.

The thickness of the retinal layers was measured in light micrographs; the number of photoreceptor cell bodies per 100 μm was estimated by superimposing a cross on the outer nuclear layer, counting cell bodies that intersected the vertical and horizontal arms of the cross, and then multiplying those values together. Histological assessments were made on one eye each of a total of 24 rats from the control, 50/10 model and 75 model groups at one of two ages, P20-21 ($n = 14$) or P31 ($n = 10$), which roughly corresponded to the age of greatest vasculopathy and of near-complete involution, respectively. For each measurement, median five sections were evaluated.

Analysis of sections from whole eyes

After sacrifice of the rat, whole eyes were enucleated (with an orienting suture) and placed immediately in 4% paraformaldehyde where they were fixed for 24 h. After fixing, they were embedded in paraffin and sectioned (25 μm) vertically, parallel to the

anteroposterior axis of the eye. Sections through the sagittal plane were selected by the appearance of the optic nerve exiting the posterior of the eye. These were mounted on slides, stained with hematoxylin and eosin to reveal structure, photographed using bright-field microscopy (DM5500) and montaged as above (Photoshop CS3).

After review of the Hughes schematic eye for rat [23], the following assumptions were developed: (1) A cross section of the rat eye is well approximated by a circle (<2% "wider" than "deep"); as a corollary, the rat eye is a sphere. (2) A reconstruction of the main features of the whole eye can be generated by rotating a pupil/optic nerve cross section around the axis of the eye, allowing derivation of, for instance, the full surface area of the retina using simple geometry. The circumference of the eye was traced and measured (ImageJ) in two parts: an anterior arc (mostly the cornea) from one point of iris attachment to the other ("the angles") and a posterior arc (mostly the sclera) from the same two points; this latter measurement closely approximated the length of the retina from inferior to superior edges of the *ora serrata*. From the length of these arcs and the circumference of the eye (their sum), three parameters of eye size based on Robb [24] were derived as shown in Fig. 2: (1) The axial length (diameter of the sphere, d), (2) the diameter of the circle formed by the *ora serrata* (o), and (3) the distance from (and perpendicular to) the plane of the *ora serrata* to the
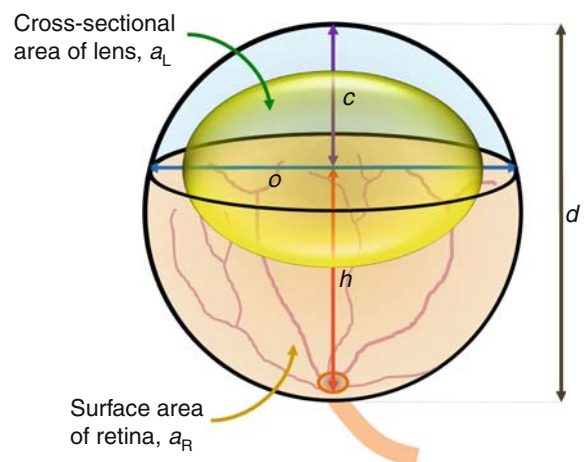

Fig. 2 Schematic eye showing features derived from measurements on sagittal anteroposterior cross sections of the eye

back of the eye (h); h is approximately equal to the posterior nodal distance. In addition, the distance from the plane of the *ora serrata* to the apex of the cornea (c) and the surface area of the retina (a_R) were calculated. Finally, the cross-sectional area of the lens (a_L) was also traced and measured (ImageJ). Parameters of the structure of the eye were derived from measurements made on eyes of three each of 50/10 model, 75 model and control rats at P19-20.

To confirm that our measurement technique produced reasonable estimates of the ratio of anterior to posterior retinal distances, we downloaded the PDF of Hughes' manuscript [23] from Science Direct (Elsevier, Amsterdam, The Netherlands) and exported the schematic eye (Hughes' Fig. 4) to a high-resolution (600 ppi) file readable by ImageJ (PNG format). We then measured the anterior and posterior arcs as described above and scaled the results by the calibration bar included in the image. We arrived at a retinal diameter of 6.31 mm, which differed by <1% from the value given in the figure (6.29 mm). The ratio of the anterior (c) to the posterior (h) retinal distances in Hughes' eye is 0.424.

Data analyses

All parameters were evaluated by ANOVA with a group factor (50/10 model, 75 model, control). Additional factors (e.g., age, region, layer) are noted in the corresponding section of the results. Post hoc testing was performed using Tukey's honestly significant difference (q) statistical test. The significance level (α) for all tests was $P < 0.05$.

Results

The retinal vessels in OIR

As shown in Fig. 3, at every age studied, the retinae in the control rats were fully vascularized all the way to the *ora serrata*. However, both OIR models often had marked areas of AR at P15 and P19, although the retinae were fully covered (or nearly so) in every P30 rat regardless of oxygen history. Broadly, AR fell into two qualitative categories: peripheral AR where the retina extended beyond the range of the major retinal arterioles and venules, and wide blocks of nonperfused retina surrounding the major retinal arterioles;

this latter category of AR was found both posteriorly and peripherally. Figure 4a plots the percentage of posterior and peripheral AR and the percentage of AR in the whole retina (a weighted average). Interestingly, the total percent of AR was approximately the same at P15 and P19 in the 75 model, but was largest at P19 in the 50/10 model, indicating that vaso-obliteration continues for some days after cessation of exposure to abnormal oxygen in the 50/10 model. The OIR rats had significantly more AR than the controls ($F = 7.28$; $df = 2,35$; $P = 0.002$) and AR was highest at the P19 test ($F = 4.53$; $df = 2,35$; $P = 0.018$). The eccentricity of greatest AR also differed between the two OIR models ($F = 8.90$; $df = 2,35$; $P = 0.001$); the percent AR was approximately balanced in the 75 model across posterior ($\sim 10\%$ at P19) and peripheral ($\sim 9\%$ at P19) retina, but was much lower in posterior ($\sim 1\%$ at P19) than peripheral ($\sim 29\%$ at P19) retina in the 50/10 model.

Inspection of the flatmounts from the 30 rats whose retinae had orientation information from fundus images revealed that AR tended to be prevalent in the six superior CH rather than the six inferior CH ($F = 5.09$; $df = 1,21$; $P = 0.035$), although, across all groups and ages, some AR was found in all twelve CH (not shown).

As shown in Fig. 4b, the group by age pattern for the occurrence of NV broadly mirrored that for AR, with NV in the 75 model fairly stable across the two early tests (P15, P19) and 50/10 rats having the most severe retinopathy ($F = 5.37$; $df = 2,35$; $P = 0.009$) at P19, followed by nearly complete recovery ($F = 4.46$; $df = 2,35$; $P = 0.019$) at P30 in both OIR models. At the P15 and P19 tests, NV was observed in every 50/10 model rat but in only six out of ten 75 model rats. Linear regression through the OIR rats' data indicated that every 6–7% additional AR was associated with the spread of NV to an additional clock hour ($r = 0.875$; $P < 0.001$). NV was nearly always found in the peripheral retina. In contrast to the AR data, in the subset of retinae that could be oriented by reference to fundus images, there was no significant effect of superior versus inferior retina on CH of NV.

However, even though both AR and NV disappeared by the P30 observation, a closer inspection of the capillaries in the OIR models revealed that the caliber of ROP rats' fine vasculature remained narrow relative to controls (bottom panels of Fig. 3) as has

Fig. 3 Sample flatmounted retinae of 50/10 model, 75 model and control rats at the three test ages (*to left*). *Calibration bars* are 1 mm. The boundary between posterior and peripheral retina is shown (*circle*). Whole retinae from P15 rats are shown in the *top panels*. A single quadrant is selected and presented at higher magnification (see *calibration bar*) in the second, third and fourth rows. From the P30 data, a 0.3 mm^2 region is selected from each of the P30 images (*white box*) and shown at the highest magnification in the bottom row
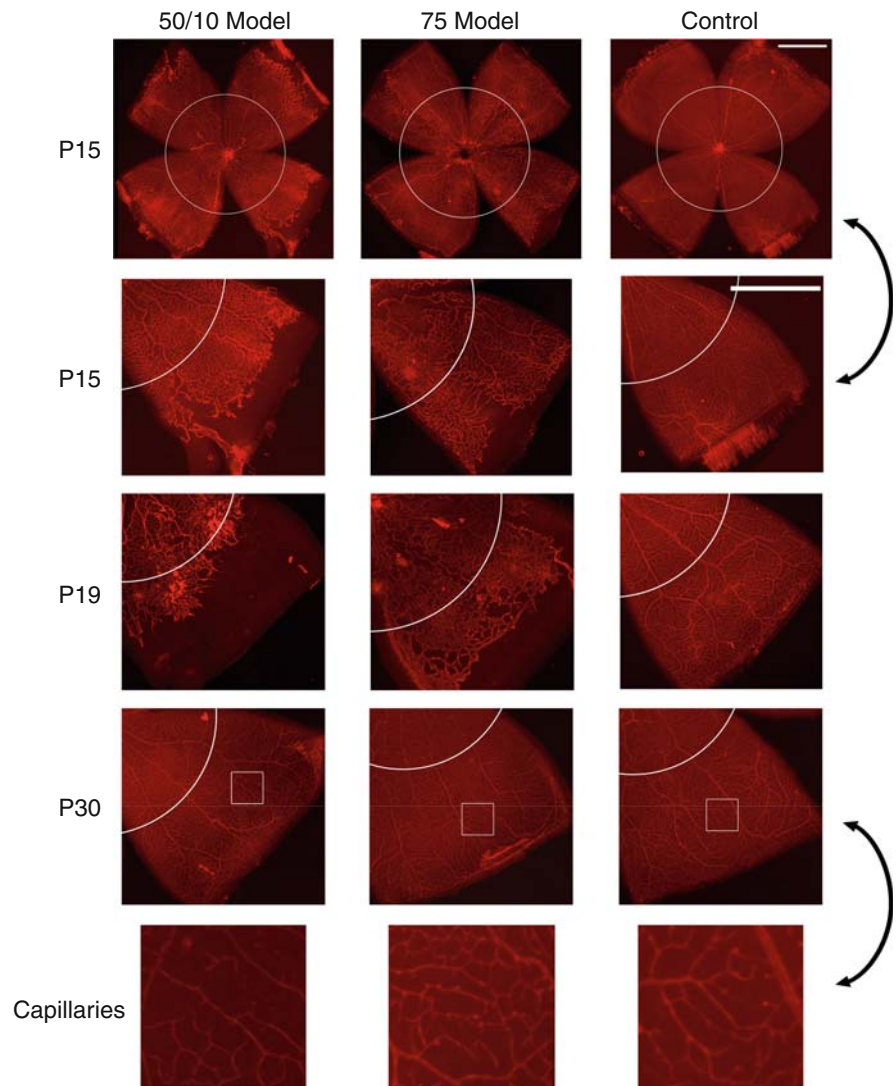
been seen in the retinae of adult humans with a history of ROP [25].

The retinal layers in OIR

As shown in Fig. 5a, the thicknesses of seven retinal layers were included in the analyses: the rod outer segments (ROS), rod inner segments (RIS), outer nuclear layer (ONL), outer plexiform layer (OPL), inner nuclear layer (INL), inner plexiform layer (IPL), and ganglion cell layer (GCL). The histological data were analyzed two ways: for posterior versus peripheral differences and for superior versus inferior differences. Because of this double analysis, α was adjusted to 0.025 for these tests.

Across all measurements, in control rats, the average thickness of the retina was approximately 215 μm, although, when the data were sorted by eccentricity (posterior versus peripheral) the posterior retina was slightly, but significantly ($F = 10.0$; $df = 1,18$; $P = 0.005$), thicker than the peripheral retina (~ 225 and 205 μm, respectively). Figure 5b plots the thicknesses of the retinal layers, averaged across eccentricity, from histological sections taken from immediately superior and inferior to the ONH (posterior retina) and from the periphery for 50/10 model, 75 model and control rats. As there were no significant main or interaction effects of age, the data are pooled across the two test ages (P20-21, P31). The 50/10 model rats' retinae were significantly

Fig. 4 Mean + SEM Vascular parameters plotted at the three test ages. a Percent of retinal area devoid of capillaries at the posterior pole and the periphery, and in total. b Number of clock hours containing neovascularization
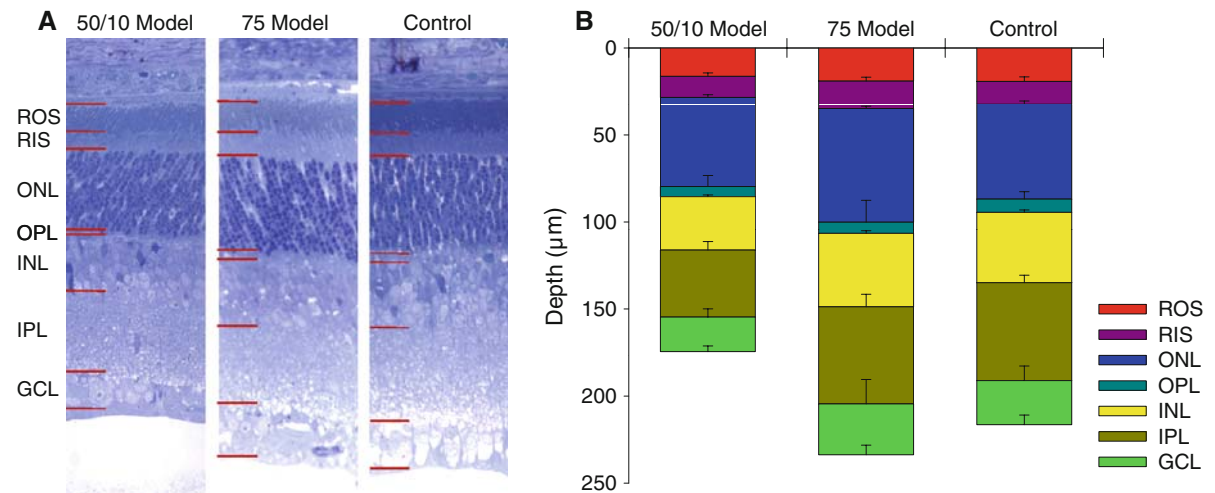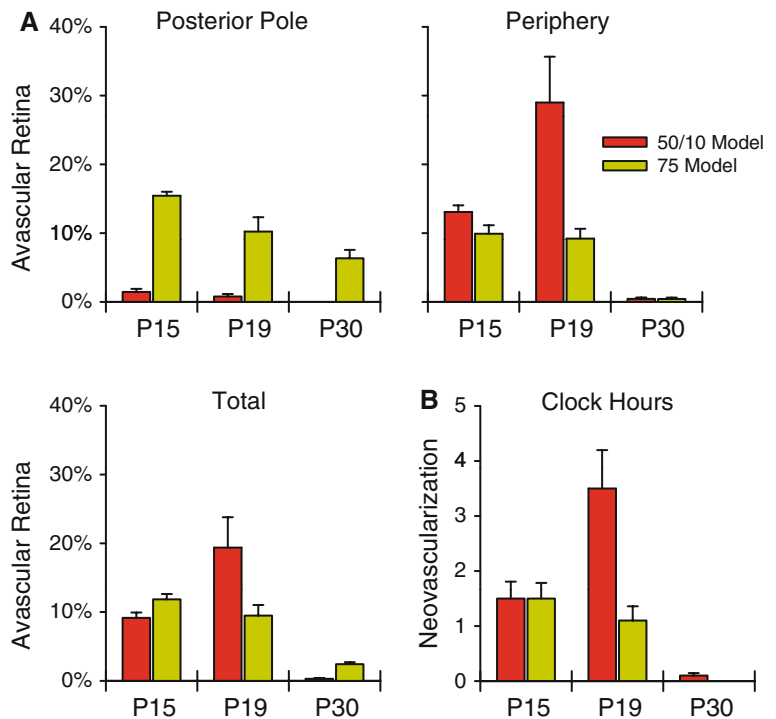

Fig. 5 The layers of the neural retina. a 100 μm wide cross sections from a 50/10 model, a 75 model and a control rat taken from just inferior to the ONH (0.5–1.0 mm eccentric) at P20–21. *Red lines* indicate approximate boundaries between the retinal layers: the rod outer segments (ROS), rod inner segments (RIS), outer nuclear layer (ONL), outer plexiform layer (OPL), inner nuclear layer (INL), inner plexiform layer (IPL), and ganglion cell layer (GCL). b Mean retinal depth (and SD of *thickness*) of the layers. The retina in 50/10 model rats is significantly thinner than in controls; the 75 model did not differ significantly

($F = 9.84$, $df = 2,21$; $P = 0.001$) thinner (~ 185 μm posterior and ~ 164 μm peripheral) than the control rats' and the 75 model rats'. The 75 model rats did not differ significantly from controls. There was no significant effect of region when the data were sorted

by inferior versus superior retina (not shown). Post hoc evaluation of the changes in individual retinal layers revealed that it the postreceptor layers (OPL, INL, IPL, GCL) that were significantly thinner in the 50/10 model than in controls. The thicknesses of the

photoreceptor layers (ROS, RIS, ONL) were not significantly altered by OIR.

The ONL nuclei counts were used to estimate the number of photoreceptors in the retina as detailed in the following section.

Effects of OIR on the growth of the eye

The small samples ($n = 3$) of ocular measurements obtained in 50/10 model, 75 model and control rats did not permit statistical evaluation, but key features of the results are shown in Fig. 6. The 50/10 model and 75 model rats' eyes were smaller than the eyes in the controls; derived mean volumes were, respectively, 38.7, 38.5, and 44.0 mm^3. These values, even in the controls, were somewhat smaller than the value given by Hughes [23]; however, these rats were younger (P19-20 versus Hughes' P115-130) and these eyes were fixed. The cross-sectional area of the lens, a_L, was similarly smaller in the 50/10 model (3.90 mm^2) and 75 model (3.86 mm^2) rats than in controls (4.17 mm^2). As shown in Fig. 6b, the ratio of the anterior (c) to the posterior (h) retinal distances differed between the OIR models and controls. The ratio measured in our control rats (mean 0.450) agreed reasonably well with the value of 0.424 derived from Hughes' schematic eye [23]. Correspondingly, the diameter of the circle formed by the *ora serrata*, o, was smallest in the 50/10 model rats, intermediate in 75 model rats, and largest in the controls.

The surface area of the retina, a_R, was estimated from $dh\pi$. The relative shift in the plane of the *ora serrata* (Fig. 6b) resulted in a_R being almost constant across the 50/10 model (41.3 mm^2), 75 model

(40.2 mm^2), and control (41.3 mm^2) rats. These values were in fair agreement with estimates of retinal surface area derived from the P19 retinal flatmounts (respectively, 35.6, 43.1, and 45.8 mm^2), although there were variations as great as $\sim 15\%$ in the 50/10 model.

The total number of photoreceptors in the retinae of rats from which histologic sections were taken was estimated by averaging the ONL nuclei counted in the 100 μm sections (Fig. 5) across the four measured regions (superior versus inferior, posterior versus peripheral), dividing by 100 and squaring to obtain a density measure (nuclei μm^{-2}), and multiplying that value by the average retinal area determined for that group and age from the retinal flatmounts. The calculated number of photoreceptors were (median) 25.2 million in the 50/10 model, 22.6 million in the 75 model, and 24.4 million in controls (in good agreement with stereological assessments of photoreceptor number [26]). Despite the large number of assumptions in this analysis, these data provide no evidence of substantial dropout of photoreceptors in the ROP rat retina.

Discussion

Marked vascular abnormalities characterized both the 50/10 model and 75 model ROP rats at younger ages (P15, P19), as did near-complete vascular recovery by P30. Large regions lacking capillary coverage were observed in every flatmounted retina of an ROP rat through the P19 test. However, avascular regions were almost completely absent in control rats, indicating that either vaso-obliteration or delayed
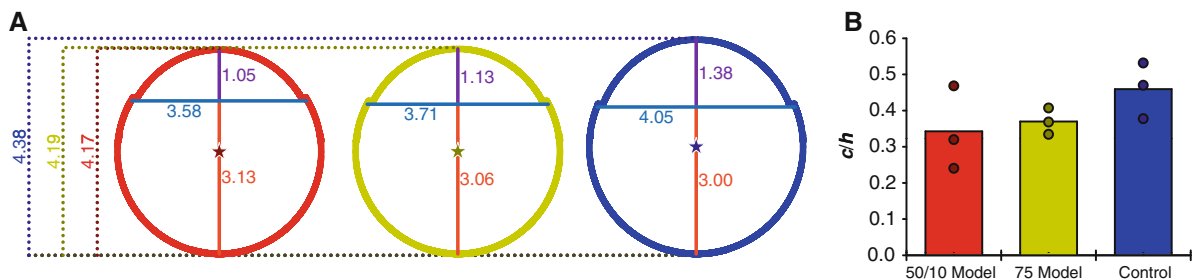

Fig. 6 Anatomic measures of the rat eye at P19-20 for 50/10 model (*red*), 75 model (*yellow*) and control (*blue*) rats. **a** In millimeters, the mean axial length (*d*, *stippled lines*), diameter of the circle formed by the *ora serrata* (*o*, *blue lines*), distance from the cornea to the plane of the *ora serrata* (*c*, *purple lines*), and height of the retina from ONH to the plane of the *ora serrata* (*h*, *orange lines*), are given and drawn to scale. The center of the eye is indicated by a *star*. **b** Mean (*bars*) and individual (*points*) ratios of the anterior (*c*) to posterior (*h*) distances

angiogenesis occurs in both ROP models. Indeed, some vaso-obliteration must occur in the 50/10 model as their retinae were more avascular 5 days after the last abnormal oxygen exposure (P19) than immediately following induction of OIR (P15).

Neovascularization was likewise most prominent in the OIR models at P19, although it occurred only sporadically, even then, in the 75 model rats. Thus, unlike in the mouse pup wherein a similar exposure to continuous high oxygen reliably produces NV [27], the exposure of the infant rat to continuous high oxygen does not. In contrast, the alternating oxygen exposure of the 50/10 model did produce NV in every flatmount studied through P19, in agreement with previous reports [18]. Differences in the response of the retina to alterations in inspired oxygen are found not just between murine species, but also between species strains [28–30].

AR was significantly more likely to occur in inferior rather than superior CH, in contrast to light damage [31]. Overall, increasing percentages of AR were correlated with increasing CH of NV. Therefore, it might be anticipated that NV would also be more prevalent inferior. However, this was not found. It has been suggested [32] that light serves to reduce the metabolic demands of the rod photoreceptors, and, indeed, the overhead track lighting of our animal colony would necessarily more directly illuminate the inferior retina. Perhaps lower rod demands in inferior retina consequently elicited a weaker pro-angiogenic retinal response resulting in a paucity of physiological vascularization and also to *proportionately* (as related to local AR) lower incidence of NV.

We note that the nearly complete recovery of AR and NV in the OIR rats is consistent with the previously reported [5, 6] recovery in the tortuosity of the superficial retinal vessels. However, in those reports, it was also observed that the blood vessels in the 75 model rats remain more tortuous than those in controls, even to adulthood. Vasculopathy, defined by the occurrence of NV, was more severe in the 50/10 model than in the 75 model in this report. An explanation for this discrepancy might lie in the histological data from the neural retina: The postreceptor retina was markedly thinned in 50/10 model rats (Fig. 5). A "back-of-the-envelope" calculation of postreceptor retinal volume, arrived at by multiplying the mean aggregate thicknesses of the postreceptor retinal layers (OPL-GCL) by the mean size in each group of a flatmounted retina for

the P19-20 rats, indicated that the size of the postreceptor space was $\sim 40\%$ smaller in 50/10 model rats than in 75 model rats or controls. Recovery of postreceptor function, as assessed by ERG, has been shown to go hand-in-hand with recovery of the superficial blood vessel abnormalities [5, 33] and with expression of molecular growth factors [7] that mediate vascular and neural remodeling [34]. If, in this instance of tightly intermingled systems, neural remodeling and vascular remodeling are inseparable due to their reliance on shared growth factors [35], then, in the 50/10 model, the postreceptor retina's putative effort to salvage retinal function may have led to concomitant vascular remodeling. This would not occur to the same extent in the 75 model rats.

A similar back-of-the-envelope calculation of the volume of the photoreceptor layers (ROS-ONL) in the ROP models and controls found an $\sim 22\%$ reduction in the size of the photoreceptor space in 50/10 model rats relative to controls. This reduction was very similar to the reduction in rod response amplitude ($\sim 23\%$ at P19-P31) previously reported (Akula et al. [5], Table 1, Rm_{P3}) in this model. Likewise, the reduction in the postreceptor space was similar to the reduction in the amplitude of the bipolar cell response ($\sim 50\%$, Vm) and summed amplitude of the ERG oscillatory potentials ($\sim 54\%$, Akula et al. [33], Table 1, $SOPA$) at the same ages. Thus, the anatomic abnormalities observed in the 50/10 model rats have a functional correlate. Interestingly, though, this was *not* true for the 75 model rats, whose neural retinae had no obvious structural defects, but whose ERG responses indicated reduction in receptor ($\sim 21\%$) and bipolar cell ($\sim 33\%$) response amplitudes [5]; although it should be noted that the oscillatory potentials in 75 model rats were normal [33].

References

1. Gilbert C (2008) Retinopathy of prematurity: a global perspective of the epidemics, population of babies at risk and implications for control. Early Hum Dev 84(2):77–82

2. Hussain N, Clive J, Bhandari V (1999) Current incidence of retinopathy of prematurity, 1989–1997. Pediatrics 104(3): e26

3. Early Treatment for Retinopathy of Prematurity Cooperative Group (2003) Revised indications for the treatment of retinopathy of prematurity: results of the early treatment for retinopathy of prematurity randomized trial. Arch Ophthalmol 121(12):1684–1694

4. Reynaud X, Hansen RM, Fulton AB (1995) Effect of prior oxygen exposure on the electroretinographic responses of infant rats. Invest Ophthalmol Vis Sci 36(10):2071–2079

5. Akula JD et al (2007) Rod photoreceptor function predicts blood vessel abnormality in retinopathy of prematurity. Invest Ophthalmol Vis Sci 48(9):4351–4359

6. Liu K et al (2006) The retinal vasculature and function of the neural retina in a rat model of retinopathy of prematurity. Invest Ophthalmol Vis Sci 47(6):2639–2647

7. Akula JD et al (2008) The neurovascular relation in oxygen-induced retinopathy. Mol Vis 14:2499–2508

8. Fulton AB et al (2009) Retinal degenerative and hypoxic ischemic disease. Doc Ophthalmol 118(1):55–61

9. Dorfman AL et al (2009) The effect of oxygen and light on the structure and function of the neonatal rat retina. Doc Ophthalmol 118(1):37–54

10. Fielder AR, Quinn GE (1997) Myopia of prematurity: nature, nurture, or disease? Br J Ophthalmol 81(1):2–3

11. Crewther SG et al (2006) Ionic control of ocular growth and refractive change. Proc Natl Acad Sci USA 103(42): 15663–15668

12. Quinn GE et al (1992) Development of myopia in infants with birth weights less than 1251 grams. The Cryotherapy for Retinopathy of Prematurity Cooperative Group. Ophthalmology 99(3):329–340

13. Quinn GE et al (1998) Prevalence of myopia between 3 months and 5 1/2 years in preterm infants with and without retinopathy of prematurity. Cryotherapy for Retinopathy of Prematurity Cooperative Group. Ophthalmology 105(7):1292–1300

14. O'Connor AR et al (2002) Long-term ophthalmic outcome of low birth weight children with and without retinopathy of prematurity. Pediatrics 109(1):12–18

15. Cook A et al (2003) Ocular growth and refractive error development in premature infants without retinopathy of prematurity. Invest Ophthalmol Vis Sci 44(3):953–960

16. O'Connor AR et al (2006) Change of refractive state and eye size in children of birth weight less than 1701g. Br J Ophthalmol 90(4):456–460

17. Cook A et al (2008) Ocular growth and refractive error development in premature infants with or without retinopathy of prematurity. Invest Ophthalmol Vis Sci 49(12): 5199–5207

18. Penn JS et al (1995) The range of PaO$_2$ variation determines the severity of oxygen-induced retinopathy in newborn rats. Invest Ophthalmol Vis Sci 36(10):2063–2070

19. Penn JS, Henry MM, Tolman BL (1994) Exposure to alternating hypoxia and hyperoxia causes severe proliferative retinopathy in the newborn rat. Pediatr Res 36(6): 724–731

20. Penn JS, Tolman BL, Lowery LA (1993) Variable oxygen exposure causes preretinal neovascularization in the newborn rat. Invest Ophthalmol Vis Sci 34(3):576–585

21. Penn JS, Tolman BL, Henry MM (1994) Oxygen-induced retinopathy in the rat: relationship of retinal nonperfusion to subsequent neovascularization. Invest Ophthalmol Vis Sci 35(9):3429–3435

22. Banin E et al (2006) T2-TrpRS inhibits preretinal neovascularization and enhances physiological vascular regrowth in OIR as assessed by a new method of quantification. Invest Ophthalmol Vis Sci 47(5):2125–2134

23. Hughes A (1979) A schematic eye for the rat. Vision Res 19(5):569–588

24. Robb RM (1982) Increase in retinal surface area during infancy and childhood. J Pediatr Ophthalmol Strabismus 19(4):16–20

25. Hammer DX et al (2008) Foveal fine structure in retinopathy of prematurity: an adaptive optics Fourier domain optical coherence tomography study. Invest Ophthalmol Vis Sci 49(5):2061–2070

26. Mayhew TM, Astle D (1997) Photoreceptor number and outer segment disk membrane surface area in the retina of the rat: stereological data for whole organ and average photoreceptor cell. J Neurocytol 26(1):53–61

27. Smith LE et al (1994) Oxygen-induced retinopathy in the mouse. Invest Ophthalmol Vis Sci 35(1):101–111

28. van Wijngaarden P et al (2007) Genetic influences on susceptibility to oxygen-induced retinopathy. Invest Ophthalmol Vis Sci 48(4):1761–1766

29. van Wijngaarden P et al (2007) Kinetics of strain-dependent differential gene expression in oxygen-induced retinopathy in the rat. Exp Eye Res 85(4):508–517

30. van Wijngaarden P et al (2005) Strain-dependent differences in oxygen-induced retinopathy in the inbred rat. Invest Ophthalmol Vis Sci 46(4):1445–1452

31. Tanito M et al (2008) Topography of retinal damage in light-exposed albino rats. Exp Eye Res 87(3):292–295

32. Arden GB et al (2005) Spare the rod and spoil the eye. Br J Ophthalmol 89(6):764–769

33. Akula JD et al (2007) The oscillatory potentials of the dark-adapted electroretinogram in retinopathy of prematurity. Invest Ophthalmol Vis Sci 48(12):5788–5797

34. Jones BW et al (2003) Retinal remodeling triggered by photoreceptor degenerations. J Comp Neurol 464(1):1–16

35. Klagsbrun M, Eichmann A (2005) A role for axon guidance receptors and ligands in blood vessel development and tumor angiogenesis. Cytokine Growth Factor Rev 16(4–5): 535–548